Nanoscale Characterization of a Novel Electro-Chemical Memory Device by STEM-EELS

Stephen D Funni, Longlong Xu, Bilge Yildiz, Judy Cha

Microscopy and Microanalysis, **30** (Suppl 1), 2024, 1130–1132
https://doi.org/10.1093/mam/ozae044.562

Microscopy AND Microanalysis

Meeting-report

Nanoscale Characterization of a Novel Electro-Chemical Memory Device by STEM-EELS

Stephen D. Funni[1], Longlong Xu[2], Bilge Yildiz[2], and Judy Cha[1]

[1]*Department of Materials Science and Engineering, Cornell University, Ithaca, New York, USA*
[2]*Department of Materials Science and Engineering, Massachusetts Institute of Technology, Cambridge, Massachusetts, USA*

Analog resistive memory devices have been proposed as a pathway to accelerated, energy-efficient training and implementation of deep learning in a physically implemented neural network [1]. Resistive memory technologies, such as phase change and conductive filament devices, have been demonstrated as potential routes to neuro-inspired computing, but have drawbacks in reliability and power consumption. Recently, hydrogen-based electro-chemical random access memory (EC-RAM), has been shown to overcome these issues [2, 3]. Using a WO_3 channel, proton-based EC RAM devices are capable of conductance modulation over three orders of magnitude with 1000 or more discernable states, making them well suited to analog neuro-morphic computing applications [3]. An EC-RAM device and its working principle are illustrated in Figure 1a.

To continue to improve and develop EC-RAM devices, the microstructure of the device materials and their interfaces must be understood, including the evolution during repeated cycling. We perform scanning transmission electron microscopy (STEM) imaging and electron energy loss spectroscopy (EELS) studies of as-grown and cycled devices using a Thermo-Fisher Scientific Spectra microscope. Imaging is done at 300 kV while EELS experiments are conducted at 120 kV. Figure 1b shows a typical high-angle annular dark field (HAADF) STEM image of the gate/electrolyte/channel device stack deposited on SiO_2. We find that the HfO_2 electrolyte contains both nanocrystalline and amorphous regions with a high density of nano-pores distributed throughout the layer. An interconnected pore structure is critical to facilitating proton conduction via functionalized interior pore surfaces. The many large pores observed at the electrolyte/channel interface, however, are detrimental to device operation by reducing the interface area for ion conduction into the channel and consequently increasing the needed drive voltage.

EEL spectra re collected from three specimens: as-deposited (AD), lightly cycled (LC), and heavily cycled (HC) to near electrolyte breakdown. As hydrogen rapidly diffuses out of PdH_x under vacuum and is not stable in WO_3 when exposed to air, no significant spectral differences are observed in the gate or channel layers among the three samples. Figure 2a shows the oxygen K-edge spectra from the electrolyte layer of the three samples. We find that the first fine structure peak at the edge onset (attributed to e_g hybridization between the O 2p and Hf 5d orbitals) is depressed relative to spectra in literature, likely due to the significant fraction of amorphous HfO_2 in our devices [4]. Furthermore, we note a pre-edge shoulder appearing only in the HC device. We attribute the pre-edge intensity in this sample to a change in the average oxygen coordination environment, increasing the number of 4-fold over 3-fold coordinated sites (i.e. a reduction of oxygen content) [5]. A similar decrease in oxygen K-edge onset energy has also been seen in the sub-stoichiometric interface layer between Si-SiO_2 [6]. Such a chemical change is expected near electrolyte breakdown when oxygen loss occurs due to ion migration caused by a high driving voltage and/or repeated cycling. The pre-edge shoulder could also be indicative of the formation of in-gap states, which would allow electronic conduction through the electrolyte and result in device failure [6].

To discern the spatial source of the pre-edge feature, we compare the oxygen K-edge spectra from the regions of the HfO_2 layer with and without the nano-pores; We integrate our spectrum image scan from the HC device into two spectra according to the corresponding simultaneous HAADF image intensity (using a cutoff intensity that marks the presence of pores). In Figure 2c we show the spectra from the "porous" and "dense" regions thus defined. We find that the "porous" areas are responsible for the pre-edge feature seen in the overall spectra. This observation is logical since ionic mobility (both O^{2-} and H^+) is highest at the internal pore surfaces. Thus, an electronically conducting pathway could form through oxygen loss in the electrolyte and cause device failure.

Enhancements to H^+ ionic conductance, especially through improved interface quality, will help to lower driving voltages and increase device lifetime. For *in operando* studies of the EC-RAM devices to monitor potential structure evolution, *in situ* environmental TEM experiments are being conducted to identify additional possible failure modes and better understand device operation dynamics that cannot be seen through *ex situ* observation alone. These results will be discussed during the presentation [7].

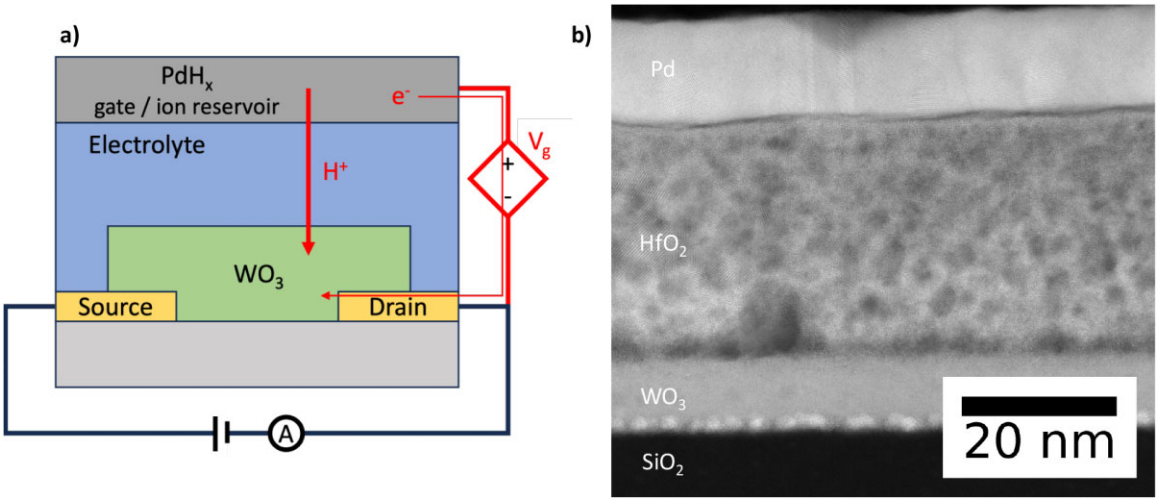

Fig. 1. a) Operational concept schematic of the EC-RAM device. The insertion of hydrogen ions to the WO_3 channel through a solid electrolyte is controlled by applying a drive voltage to the PdH_x gate, which in turn modulates the resistance state of the EC-RAM device. **b)** HAADF STEM image of the working device layers.

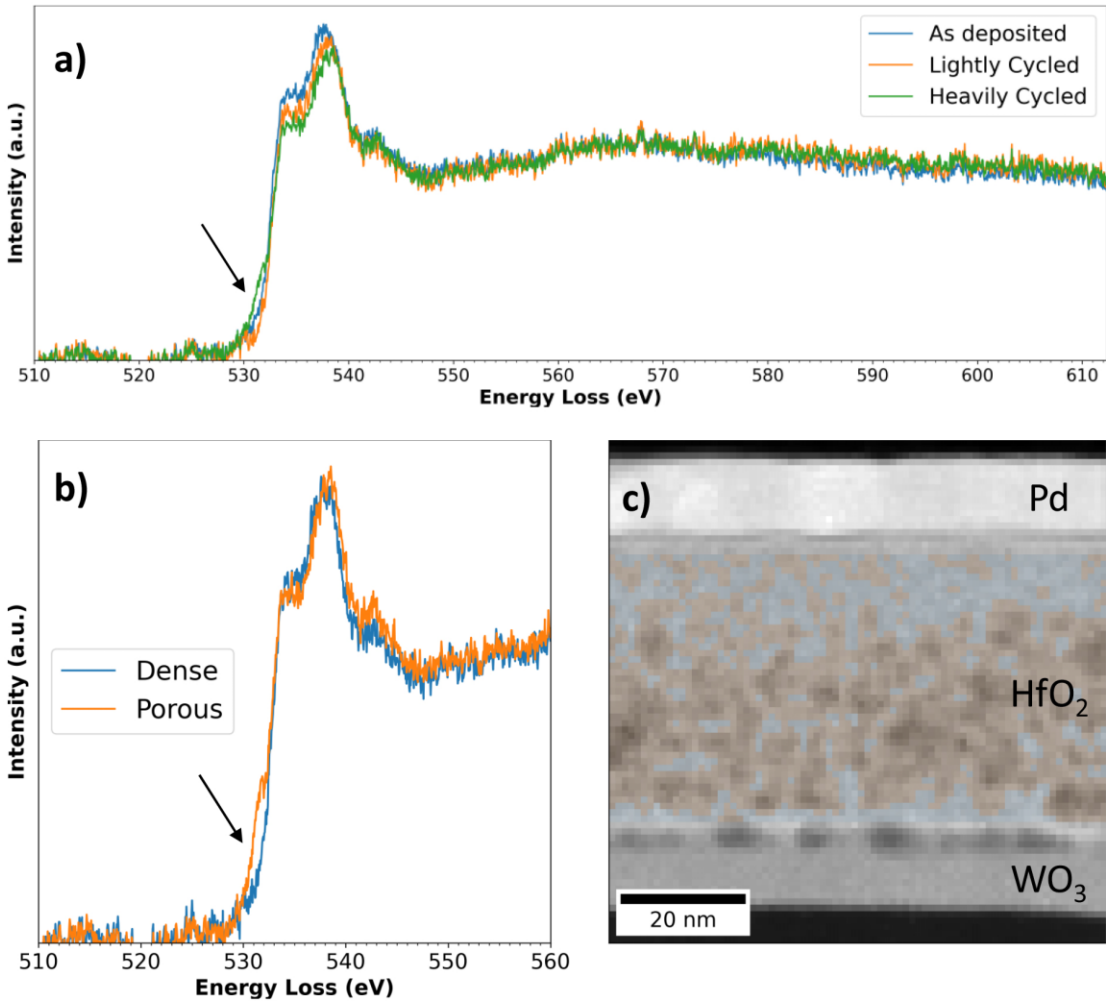

Fig. 2. a) Oxygen K-edge EEL spectra from three devices, as-deposited (AD), lightly cycled (LC), heavily cycled (HC). Note the subtle pre-edge intensity in the HC spectrum compared to the AD and LC spectra. **b)** Integrated spectra from the dense and porous regions of a representative EEL spectrum image scan. Arrows in a) and b) indicate the pre-edge intensity. **c)** The HAADF signal collected simultaneously to the EELS scan with light blue and light orange coloring overlaid to indicate the regions integrated into the dense and porous spectra in b).

References

1. T. Gokmen and Y. Vlasov, *Frontiers in Neuroscience* [Online] 10 (2016), https://www.frontiersin.org/articles/10.3389/fnins.2016.00333 (Accessed: Jan. 25, 2024.)
2. M. Huang, *et al.*, *Advanced Materials* **35** *(2022)*, p. 2205169, doi: 10.1002/adma.202205169.
3. X. Yao *et al.*, *Nature Communications* **11** (2020), 3134, doi: 10.1038/s41467-020-16866-6.
4. P. Rauwel, *et al.*, *Journal of Applied Physics* **112**, no. 10 (2012), p. 104107, doi: 10.1063/1.4766272.
5. G. D. Wilk and D. A. Muller, *Applied Physics Letters* **83**, no. 19 (2003), pp. 3984–3986, doi: 10.1063/1.1626019.
6. D. A. Muller, *et al.*, *Nature* **399**, no. 6738 (1999), doi: 10.1038/21602.
7. SD Funni and JJ Cha were funded through the Gordon and Betty Moore Foundation's EPiQS Initiative, Grant GBMF9062.1. This work made use of the electron microscopy facility of the Platform for the Accelerated Realization, Analysis, and Discovery of Interface Materials (PARADIM), which is supported by the National Science Foundation under Cooperative Agreement No. DMR-2039380, and the Cornell Center for Materials Research Shared Facilities which are supported through the NSF MRSEC program (DMR-1719875).